Generation of Whistler-Wave Heated Discharges with Planar Resonant rf Networks

Ph. Guittienne
Helyssen, CH-1092 Belmont-sur-Lausanne, Switzerland

A. A. Howling and Ch. Hollenstein
Ecole Polytechnique Fédérale de Lausanne, CH-1015 Lausanne, Switzerland
(Received 12 April 2013; published 19 September 2013)

Magnetized plasma discharges generated by a planar resonant rf network are investigated. A regime transition is observed above a magnetic field threshold, associated with rf waves propagating in the plasma and which present the characteristics of whistler waves. These wave heated regimes can be considered as analogous to conventional helicon discharges, but in planar geometry.

DOI: 10.1103/PhysRevLett.111.125005 PACS numbers: 52.80.Pi

It is well known that electromagnetic (EM) waves cannot propagate into plasmas for frequencies lower than the electron plasma frequency (typically $\omega_{pe} > 1$ GHz). It is a consequence of the fact that this medium exhibits a nonnegligible electrical conductivity. A benefit of this property was notably found in the possibility for EM waves to be transmitted across the world due to reflections on the ionosphere. On the other hand, the nonpropagation of rf fields into plasmas leads to some difficulties for the development of rf volume plasma sources because the energy deposition occurs only in a skin-depth region, typically over 1–3 cm, close to the source currents. In the case of magnetized plasmas, for which the electrons are constrained to follow a cyclotron motion, the conductivity tensor associated with the plasma is no longer diagonal and isotropic, and as a consequence it is possible for low frequency EM modes to propagate into the medium. These modes, known as the whistler waves, were first and mainly studied in the framework of atmospheric plasmas (magnetosphere and ionosphere) where they abound [1–3]. In this case, the plasma is a preexisting medium where very low frequency whistlers are generated, notably due to lightning. But whistler waves are also extremely interesting in terms of plasma generation, as shown by Boswell in the early 1970s with the development of the first helicon source [4]. Helicon discharges are characterized by high electron densities, typically 1 order of magnitude higher than conventional inductively coupled discharges, although the underlying energy deposition mechanisms are not yet well understood [5–10]. The helicon source geometry is intrinsically cylindrical as the discharge is generated in a tube with an axial static magnetic field. Specially shaped rf antennas are used to excite the whistler wave, the more popular being the Nagoya III [11], the double saddle coil [12], and the helical antenna [13]. Despite their ability to generate high density plasmas, these conventional helicon sources have not yet found a very wide range of applications because of their low versatility, notably in terms of operating pressure (typically 0.1 Pa) and with regards to the use of electronegative gases. A cylindrical resonant network, or birdcage coil, was shown to be a very efficient alternative antenna design for helicon wave excitation [14], with extended operation parameters. These improved performances are in a large part due to the fact that the birdcage coil is not only efficient for the wave excitation, but also in terms of inductive coupling, which produces the critical electron densities necessary to transit toward wave heated regimes.

Here we report the generation of whistler-wave heated discharges in a totally different geometry from the helicon source. Instead of a cylindrical antenna, we used a planar resonant rf network [15], with a static magnetic field perpendicular to the source plane. Planar resonant rf networks were already used to produce inductively coupled plasmas over a large area. The rf source being placed in a large vacuum chamber, the generated plasma is not radially bounded by a dielectric tube as in helicon discharges. It is shown that, above a given magnetic field threshold, wave heated regimes are obtained, characterized by the formation of a plasma beam extending from the source up to the end of the vacuum chamber. High electron densities (typically 10^{17} m^{-3}) have been measured for moderate levels of rf power (300 W) and magnetic field strength (30 G). We show that the excited waves present the characteristics expected for whistler waves.

We refer here to the theory of linear whistler modes that arise from the model of a uniform plasma, uniformly magnetized, for which a linearized form of the Boltzmann momentum conservation equation is used to define the medium conductivity tensor. Assuming a harmonic temporal dependence $e^{-i\omega t}$ for the first order physical quantities, and taking the static magnetic field to be oriented in the z direction, it can be shown from Maxwell equations that the transverse rf electric (or magnetic) field into the plasma must be of the form

$$\begin{aligned} E_x &= (f_1 e^{-ik_1 z} + f_2 e^{ik_1 z}) + (f_3 e^{-ik_2 z} + f_4 e^{ik_2 z}), \\ E_y &= -i(f_1 e^{-ik_1 z} + f_2 e^{ik_1 z}) + i(f_3 e^{-ik_2 z} + f_4 e^{ik_2 z}). \end{aligned} \quad (1)$$

The wave numbers $k_{1,2}$ are given by the following dispersion relation:

$$k_{1,2}^2 = \frac{\omega^2}{c^2}\left(1 + \frac{i\omega_{pe}^2}{\omega[\nu - i(\omega \pm \omega_{ce})]}\right), \quad (2)$$

where $\omega_{pe}^2 = n_e q^2/\epsilon_0 m_e$ and $\omega_{ce} = qB_0/m_e$, c being the speed of light in free space, q the magnitude of elementary charge, m_e the electron mass, n_e the plasma electron density, ϵ_0 the permittivity of free space, B_0 the static magnetic field algebraic value, and ν an effective collision frequency [16] for electrons which comprises both collisional and stochastic contributions ($\nu = \nu_m + \nu_{\text{stoch}}$).

$f_{1,2,3,4}$ are functions of (x, y) only and are to be determined by defining the boundary conditions. The longitudinal component of the electric field E_z is also only a function of (x, y) in this simple model. In a collisionless approach ($\nu = 0$) and with negligible displacement current (which is justified when $\omega \ll \omega_{pe}$), the dispersion relation (2) becomes

$$k_{1,2}^2 \approx -\frac{\omega\omega_{pe}^2}{c^2(\omega \pm \omega_{ce})}. \quad (3)$$

If B_0 is positive ($\omega_{ce} > 0$), k_1 is purely imaginary (no propagation), while for k_2 a cutoff in the propagation is expected for $\omega > \omega_{ce}$. For negative B_0, the opposite situation arises for k_1 and k_2. Considering now the general expression for the transverse components (E_x, E_y) of the electric field (1), one can see that it is circularly polarized, left- or right-handed depending on the sign of B_0. For a given time the transverse field is then characterized by a helical structure along z.

The experimental setup used for this study is presented in Fig. 1. The plasma source [fig. 1(a)] is an 11 leg planar resonant network (20×20 cm^2) [15]. The antenna legs acting essentially as inductors, this parallel L, C arrangement exhibits a set of $N - 1$ resonant frequencies, N being the number of legs, each corresponding to a normal mode for the network current distribution. Under resonance all the currents oscillate temporally in phase and are spatially sinusoidally distributed, the number of periods over the antenna being $m/2$, where $m = [1, N - 1]$ is defined as the mode number. For our experiments, the network capacitors were chosen to obtain a $m = 2$ resonance at 13.56 MHz. This antenna is placed in a half-open grounded metallic box. The empty spaces in this box are approximately filled with polytetrafluoroethylene or silicone elastomer so that plasma is generated only in front of the antenna. A 1 mm thick glass plate was placed on the resonant network as a dielectric barrier between the plasma and the source.

This assembly is placed at one end of a large cylindrical vacuum chamber (1 m long, 70 cm in diameter), the plane of the antenna being perpendicular to the chamber axis [Fig. 1(b)]. A static magnetic field is generated by a pair of Helmholtz coils. Three types of diagnostics were installed to characterize the discharges and to evidence the excitation of EM waves. Ion saturation currents were measured on single tip Langmuir probes to obtain both axial and radial relative profiles of the plasma density. A 25 GHz interferometer was used to measure the line-averaged electron density at a fixed distance from the source (25 cm). Finally, a triaxial B-dot probe was applied to characterize the rf field on the chamber axis. All the results presented here were obtained with a 30 sccm argon flow and at an operating pressure of 1.1 Pa.

Figure 2 shows some typical ion saturation current profiles obtained with the axial Langmuir probe. Four of these profiles were measured at a fixed rf power (150 W) but for different static magnetic fields ($B_0 = 0$, 13, 18, and 26 G), and the last one is an example of a regime with higher rf power and field strength. With $B_0 = 0$ G the plasma is inductively coupled to the resonant network. The ionization mainly takes place in the skin-depth region and the plasma diffuses into the chamber from there. When a small

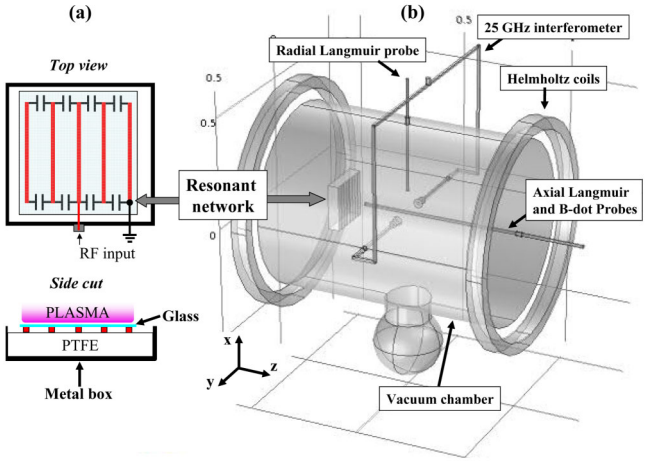

FIG. 1 (color online). (a) Schema of the rf resonant network (only five legs represented). (b) Overall experimental setup.

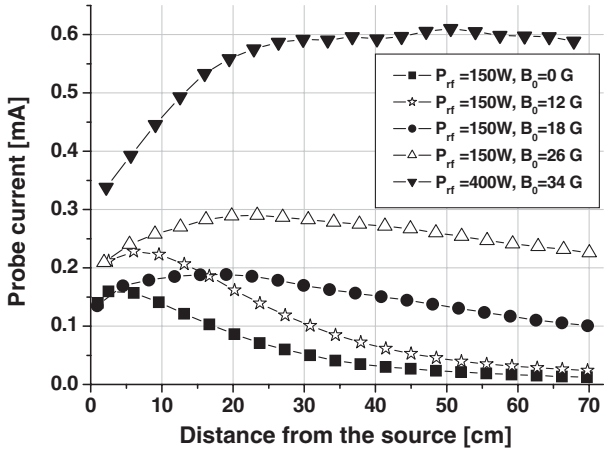

FIG. 2. Axial ion saturation current profiles measured on a single tip (length 3 mm; diameter 0.6 mm) Langmuir probe biased at −30 V.

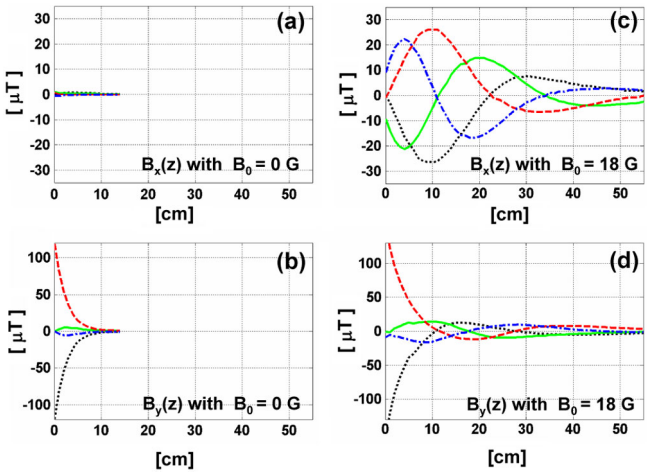

FIG. 3 (color online). Measurements of the transverse field profile [components $B_x(z)$ and $B_y(z)$] along the chamber axis at 4 times of a rf period T [$t = 0$ (full line), $T/4$ (dotted line), $T/2$ (dash-dotted line), $3T/4$ (dashed line)]. The rf input power is 100 W. (a), (b) $B_x(z)$ [$B_y(z)$] without magnetic field [inductive coupling]. (c), (d) $B_x(z)$ [$B_y(z)$] with a 18 G static magnetic field.

magnetic field is applied this diffusion profile slightly spreads along the z axis because of the electron confinement, up to a critical field value of about 15 G where a sudden regime transition is observed. This transition is characterized by an elongation of the axial density profile and is associated with the detection of rf magnetic fields far away from the source (Fig. 3). As shown in Fig. 2, with increasing rf power and magnetic field strength, flat axial density profiles extending typically 20 cm from the source up to the end of the vacuum chamber can be obtained. A diffusion from a skin-depth region close to the antenna cannot account for such density profiles which, in fact, suggest that ionization occurs quite far away from the rf network, in a totally different way than it does in purely inductive ($B_0 = 0$ G) coupling.

A comparison of the transverse magnetic field patterns measured before ($B_0 = 0$ G) and after the regime transition ($B_0 = 18$ G) is shown in Fig. 3. The transition toward a propagating wave regime is clear, and the characteristics of these waves will be further described. In the inductive regime [Figs. 3(a) and 3(b)] the field is linearly polarized and its decay is well represented by an exponential. This is expected in the framework of collisional damping ($\nu_m > \nu_{\text{stoch}}$), while for collisionless damping nonmonotonic field penetration profiles are predicted [16]. An estimation of the collision frequency for momentum transfer ν_m, using a Maxwellian electron energy distribution function with a 3 eV mean electron temperature in argon [17], leads typically to a 10 MHz value, which compared with $\omega = 85.2$ MHz indicates a moderately collisional plasma. The skin depth is measured here to be about 2 cm. This value is 1.5–2 times lower (for $\nu = 1$–100 MHz) than expected according to a conventional 1D theoretical model

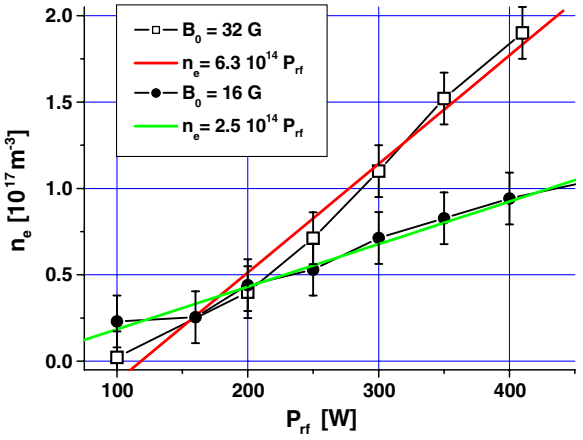

FIG. 4 (color online). Electron peak density on the chamber axis at 25 cm from the rf network as a function of the rf input power ($B_0 = 16$ G and $B_0 = 32$ G).

of the field propagation into a collisional plasma [16], but it can be shown that finite size effects can very well account for this lowered value.

The radial density profiles (not shown) measured at 25 cm from the source are peaked on the chamber axis, and can be approximated by a Gaussian (FWHM 25–30 cm). These profile measurements combined with line-averaged density measurements performed with the 25 GHz interferometer at 25 cm from the source allow the peak density on the discharge axis to be estimated. The obtained variation of the peak plasma density as a function of the rf input power is shown in Fig. 4 for $B_0 = 16$ G and $B_0 = 32$ G. Densities up to 2×10^{17} m^{-3} have been measured, and it can be seen that in the available power range the peak density varies approximately linearly with the input rf power level.

The detected propagating wave presents all the characteristics expected for whistler waves. First, as shown in Fig. 5, the transverse field has a helical structure due to an

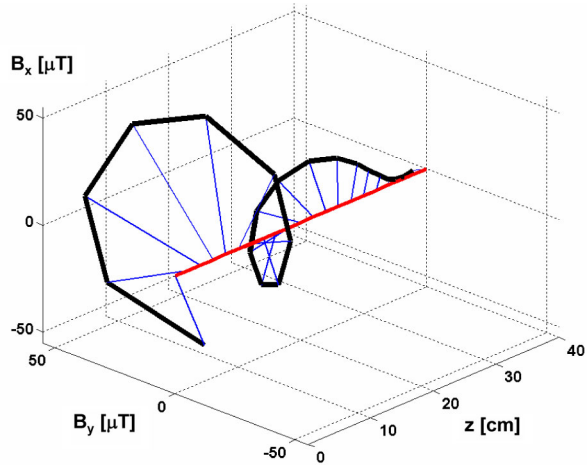

FIG. 5 (color online). Transverse rf magnetic field (B_x, B_y) as a function of z for a given time.

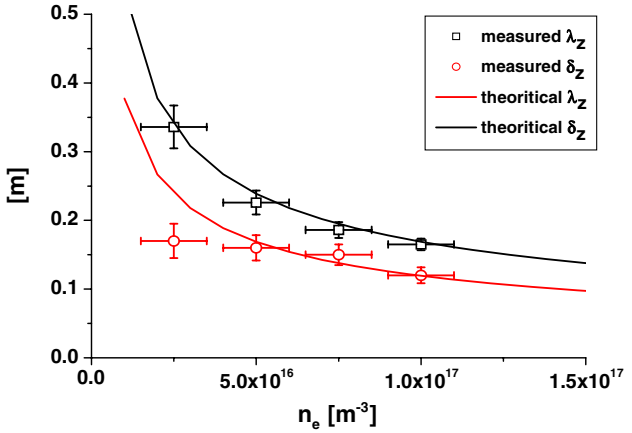

FIG. 6 (color online). Dots: Measurements of the wavelength $\lambda_z = 2\pi/\mathrm{Re}(k)$ and damping constant $\delta_z = 1/\mathrm{Im}(k)$ as a function of the peak electron density for $B_0 = 16$ G. Lines: Variations of λ_z and δ_z according to Eq. (2). The effective collision frequency ν was set to 100 MHz to account for the order of magnitude of δ_z.

elliptic polarization modulated by the propagation along z. Furthermore, the polarization of the wave is left- or right-handed depending on the sign of B_0. The measurements of the wave amplitude as a function of the static magnetic field strength (not shown) clearly demonstrate a cutoff for the propagation for $\omega > \omega_{ce}$, regardless of the power level. Finally, we have measured, as a function of the input rf power, the rf magnetic field wavelength λ_z along the z axis, as well as its damping factor δ_z, which is representative of the dissipative processes associated with the effective collision frequency ν (Fig. 6). The linear fit $n_e = 2.5 \times 10^{14} P_{\mathrm{rf}}$ obtained from Fig. 4 has been used to set the horizontal scale in Fig. 6. The full lines correspond to the expected values of λ_z and δ_z according to the dispersion relation [Eq. (2)]. The only fitting parameter introduced here is the effective collision frequency ν, which negligibly affects λ_z but has to be set to typically 100 ± 20 MHz in order to account for the measured damping constant δ_z. This last result is quite interesting. Considering the operating pressure (1.1 Pa), a 100 MHz value for ν corresponds to an effective collision rate constant K of typically 4×10^{-13} m^3/s. In the framework of a Maxwellian distribution for the electron energy [17], a mean electron temperature T_e of more than 20 eV would be necessary to account for such a rate constant by virtue of collisions only, whereas T_e was measured to be about 3.5 eV (at 25 cm from the source) with no significant variation in the available rf power range. Furthermore, if the damping of the wave was only due to collisions we would expect the effective collision frequency to be proportional to the operating pressure. But the same analysis applied to measurements (not shown) performed at 10 times lower pressure (0.1 Pa) leads to a 50 MHz effective collision frequency, only 2 times lower than for 1.1 Pa. It can be concluded that the major part of the energy dissipation in these wave heated discharges is due to stochastic contributions.

The high efficiency of planar resonant rf networks for launching whistler-wave heated discharges is certainly due to the combination of two properties. First, the rf field generated by this antenna has the correct transverse structure for the excitation of linear whistler modes, although it is linearly polarized and not circularly polarized as it should ideally be. Second, the resonant network is efficient in terms of inductive coupling, which produces the critical plasma density necessary to initiate the wave regimes. One of the major advantages of resonant networks lies in their input impedance which is high and almost purely real under resonance. This should notably allow very large planar sources to be built, avoiding the high voltages (currents) drawbacks inherent to conventional large area inductive (capacitive) sources. The generation of whistler heated discharges with a large area planar network would then lead to high density plasmas in a very large volume, which would be of prime interest for many applications. In a fundamental point of view, the theoretical understanding of the processes that sustain these wave heated discharges is still lacking. As shown here, the high effective collision frequency necessary to account for the whistler wave's damping suggests a dominant stochastic mechanism. It can reasonably be supposed that the same mechanism can be at the origin of the power deposition in helicon discharges, despite the difference in geometry, and the study of whistler heated discharges in the planar configuration could throw a new light on theoretical approaches. As an example, in the literature [5–10], short wavelength and highly damped Trivelpiece-Gould (TG) modes, which must appear in helicon discharges in order to satisfy the boundary conditions at the plasma edge, are often considered to play a central role in the rf power transfer. But in the present experiments the plasma is not radially confined as it is in helicon discharges so that TG modes damped from the plasma edge can hardly be invoked. Under the hypothesis of an equivalent energy transfer mechanism for helicons and the wave heated regimes presented here, it should be concluded that TG modes are not the main channel for the energy transfer in helicon discharges. Alternatively, under the hypothesis of a central role of TG modes in helicon sources, it should be concluded that the discharges generated by planar networks in an open geometry are sustained by a totally different energy transfer mechanism.

[1] R. A. Helliwell, *Whistlers and Related Ionospheric Phenomena* (Stanford University, Stanford, CA, 1965).
[2] R. L. Stenzel, J. Geophys. Res. **104**, 14 379 (1999).
[3] W. E. Amatucci *et al.*, Radio Sci. Bull. **319**, 32 (2006).
[4] R. W. Boswell, Phys. Lett. **33A**, 457 (1970).

[5] R. D. Tarey, B. B. Sahu, and A. Ganguli, Phys. Plamas **19**, 073520 (2012).
[6] F. F. Chen and D. D. Blackwell, Phys. Rev. Lett. **82**, 2677 (1999).
[7] F. F. Chen, Plasma Phys. Controlled Fusion **33**, 339 (1991).
[8] K. P. Shamrai, V. P. Pavlenko, and V. B. Taranov, Plasma Phys. Controlled Fusion **39**, 505 (1997).
[9] K. P. Shamrai and V. B. Taranov, Plasma Sources Sci. Technol. **5**, 474 (1996).
[10] M. Krämer, Yu. M. Aliev, A. B. Altukhov, A. D. Gurchenko, E. Z. Gusakov, and K. Niemi, Plasma Phys. Controlled Fusion **49**, A167 (2007).
[11] F. F. Chen, Phys. Plamas **3**, 1783 (1996).
[12] R. W. Boswell, Plasma Phys. Controlled Fusion **26**, 1147 (1984).
[13] D. G. Miljak and F. F. Chen, Plasma Sources Sci. Technol. **7**, 537 (1998).
[14] Ph. Guittienne, E. Chevalier, and Ch. Hollenstein, J. Appl. Phys. **98**, 083304 (2005).
[15] Ph. Guittienne, S. Lecoultre, P. Fayet, J. Larrieu, A. A. Howling, and Ch. Hollenstein, J. Appl. Phys. **111**, 083305 (2012).
[16] M. A. Lieberman and V. A. Godyak, IEEE Trans. Plasma Sci. **26**, 955 (1998).
[17] G. J. M. Hagelaar and L. C. Pitchford, Plasma Sources Sci. Technol. **14**, 722 (2005).